ACS OMEGA

Open Access

http://pubs.acs.org/journal/acsodf

Article

Evidence for the Formation of Metabolons Surrounding the Pyruvate Node in the Supercritical CO_2-Tolerant *Priestia megaterium* SR7

Nathaphon Yu King Hing, Yi Wen Kristy Chang, Ramanujam Srinivasan Vethathirri, Yulan Wang, and Janelle R. Thompson*

Cite This: *ACS Omega* 2026, 11, 33872−33880

Read Online

ACCESS | Metrics & More | Article Recommendations | Supporting Information

ABSTRACT: Carbon fixation and metabolic efficiency in extremophiles offer promising avenues for sustainable bioproduction. *Priestia megaterium* SR7 is a supercritical CO_2-tolerant extremophile, whose central carbon metabolism may be particularly well adapted toward efficient heterotrophic CO_2 fixation. However, the regulatory organization of carbon flux in this organism remains unclear, especially around the pyruvate node, a central metabolic hub that directs carbon toward energy generation, metabolic replenishment, and biosynthesis. In this work, we proposed and substantiated the formation of multiple potential metabolons, associated enzyme complexes that channel metabolites between sequential reactions, surrounding the pyruvate node in *P. megaterium* SR7, which serves as an important regulatory mechanism in central carbon metabolism by enabling the channeling of metabolites toward different pathways. Cross-linking experiments, together with subsequent proteomics, provided *in vitro* evidence of metabolon formation among phosphoenolpyruvate carboxylase (PPC), NAD+-dependent malic enzyme (NDME), lactate dehydrogenase (LDH), and pyruvate kinase (PYK) protein−protein interactions. *In silico* simulations of protein−protein interactions revealed possible interacting residues between different proteins. Furthermore, observed dilution of metabolite pools from ^{13}C isotopic labeling experiments provides *in vivo* support for metabolon formation. These insights suggested a possible novel regulatory mechanism and provided additional avenues for future metabolic engineering efforts that leverage enzyme organization to enhance CO_2-linked bioproduction.

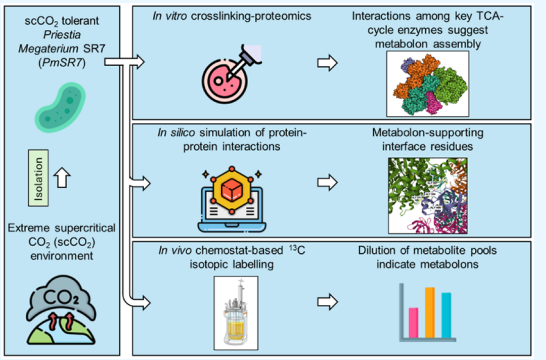

INTRODUCTION

Global energy and chemical production remain predominantly dependent on fossil resources, with over 90% currently derived from coal, natural gas, and petroleum.[1] Transitioning to sustainable biobased processes is therefore a critical challenge in addressing both energy security and climate impact. Microbial cell factories provide a promising foundation for this transition, as they can convert renewable substrates into fuels and high-value chemicals under suitable process conditions.[2] Realizing the full potential of these systems, however, requires a deeper understanding of how cellular metabolism organizes and regulates flux through key nodes to optimize efficiency and productivity.[3]

Priestia megaterium SR7 is a supercritical CO_2 ($scCO_2$) tolerant microorganism isolated from CO_2 source fields in the McElmo Dome in Colorado, USA.[4] The ability to germinate and grow in aqueous media under a $scCO_2$ headspace makes *P. megaterium* SR7 a promising biological chassis for growth under high pCO_2 and to enable exploitation of $scCO_2$ as a sustainable extraction solvent.[4,5] In comparison to conventional organic solvents, $scCO_2$ is a nonhazardous, nonflammable, and nontoxic alternative,[6] and $scCO_2$ extraction additionally offers increased extraction efficiency for many biological compounds,[7] such as oil[8] or biofuels,[9] and has the additional benefit of sterilizing most competing microorganisms via disruption of the cellular membrane,[10] thus decreasing projected operating costs. Although previous studies have characterized the physiological and genomic features of *P. megaterium* SR7 under $scCO_2$ conditions,[4,9] detailed insight into the metabolic mechanisms that enable its tolerance remains unclear.

Efficient central carbon metabolism is fundamental to microbial adaptation under environmental stress, including exposure to high pCO_2 conditions associated with $scCO_2$.[11] Given its background, we hypothesized that *P. megaterium* SR7's central carbon metabolism enzymes, such as those

Received: January 16, 2026
Revised: April 29, 2026
Accepted: May 8, 2026
Published: June 2, 2026

surrounding heterotrophic CO_2 fixation, could be substantially different than conventional model microorganisms. In particular, the pyruvate node (Figure 1), the junction between

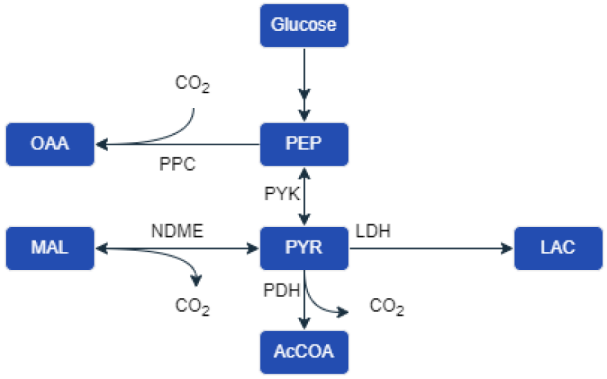

Figure 1. Overview of the pyruvate node and associated metabolic reactions relevant in this paper for Priestia megaterium SR7. The pyruvate node integrates glycolysis, the tricarboxylic acid (TCA) cycle, and anaplerotic CO_2-fixation and release pathways. Key metabolites include glucose, PEP, PYR, OAA, MAL, lactate (LAC), acetyl-coenzyme A (AcCoA), and CO_2. Enzyme abbreviations: phosphoenolpyruvate carboxylase (PPC, EC 4.1.1.31), pyruvate kinase (PYK, EC 2.7.1.40), NAD+-dependent malic enzyme (NDME, EC 1.1.1.38), pyruvate dehydrogenase (PDH, EC 1.2.4.1), and lactate dehydrogenase (LDH, EC 1.1.1.27).

glycolysis and the tricarboxylic acid cycle, is of interest because of the combined CO_2 fixating and releasing reactions mediated by phosphoenolpyruvate carboxylase (PPC), the reversible NAD+-dependent malic enzyme (NDME), and the CO_2-releasing pyruvate dehydrogenase (PDH) reaction, among other reactions. Flux through the pyruvate node is thought to be highly flexible,[12] and capable of being redirected in multiple directions. The conversion of phosphoenolpyruvate (PEP) to pyruvate normally produces ATP via pyruvate kinase (PYK), but because carbon can be rerouted through PPC, it is also possible to channel carbon toward the TCA cycle directly without generating ATP while simultaneously assimilating CO_2. Therefore, the pyruvate node represents a flexible control node that balances the carbon economy and energetic demands of the cell. To date, however, the organization and regulation of this node have not been examined in *P. megaterium* SR7 or related extremophiles.

Among the different forms of metabolic regulation, one understudied form of regulation is the formation of metabolons. Metabolons are formations of multienzyme complexes with the potential to channel metabolites from one enzyme directly or indirectly to another.[13] Close association of metabolically adjacent enzymes within a pathway allows for substrates to be efficiently or inefficiently channeled to enhance reaction rates by directly enhancing the local substrate concentration. Moreover, these channeled metabolites are shielded from potential competing pathways. For example, the formation of a carbonic anhydrase and ribulose-1,5-bisphosphate carboxylase/oxygenase (RuBisCO) metabolon in many photosynthetic organisms is a well-known phenomenon that enhances an otherwise kinetically inefficient carbon fixation process.[14]

In this work, the possibility of metabolon formation for targeted proteins surrounding the pyruvate node (Figure 1) in *P. megaterium* SR7 was investigated using a combination of *in vitro*, *in silico*, and *in vivo* approaches. Namely, protein−protein interactions were investigated using a disuccinimidyl glutarate (DSG) cross-linker, combined with subsequent proteomics, an approach previously used to characterize metabolons in the TCA cycle.[15,16] Potential protein−protein interactions were also simulated using AlphaFold 3, using common post-translational modifications detected in proteomics to investigate feasible *in silico* predictions.[17] Finally, *in vivo* evidence of metabolite channeling was obtained via isotopic labeling experiments by looking for isotopic dilution, specifically surrounding pyruvate and lactate.[18] This study demonstrated that metabolons formed around the pyruvate node act as a novel regulatory layer in *P. megaterium* SR7, revealing how spatial enzyme organization contributes to metabolic efficiency under extreme conditions and enables new avenues for metabolic engineering.

MATERIALS AND METHODS

Protein Purification of LDH, NDME, PPC, PDH, and PYK

Codon-optimized gene fragments of LDH, NDME, PPC, PDH, and PYK were purchased from Integrated DNA Technologies (United States). LDH, NDME, and PYK sequences were subcloned into the pNIC28-Bsa4 plasmid (Addgene #26103), while PPC and PDH were subcloned into pNH-TrxT (Addgene #26106) to improve protein yield. Expression plasmids were transformed into *Escherichia coli* BL21(DE3) Rosetta. Expression cultures were grown in Terrific Broth (TB) supplemented with appropriate antibiotics and 0.1% v/v antifoam 204 (Sigma-Aldrich). Briefly, 750 mL of TB was inoculated with 20 mL of overnight starter culture and incubated at 37 °C under aeration by the LEX minibioreactor system (Harbinger Biotech). Temperature was lowered to 18 °C when OD600 reached 2. A total of 0.5 mM IPTG was added after 1 h, and target protein expression continued overnight. Cells were harvested 20 h after induction by centrifugation at 4000 *g* and resuspended in at least 1.5 times the cell pellet volume of lysis buffer (100 mM HEPES, 500 mM NaCl, 10 mM imidazole, 10% glycerol, 0.5 mM TCEP, pH 8.0, supplemented with benzonase and non-EDTA protease inhibitor cocktail). Cell suspensions were sonicated on ice and clarified by centrifugation at 47000 g. Lysate supernatants were filtered and loaded onto AKTAxpress systems (Cytiva) for Ni-NTA purification, followed by size exclusion chromatography. The latter was performed on HiLoad 16/600 Superdex 75 or 200 prep grade columns (Cytiva) equilibrated in gel filtration buffer (20 mM HEPES, 300 mM NaCl, 10% (v/v) glycerol, 0.5 mM TCEP, pH 7.5). Eluted fractions were analyzed on SDS-PAGE; pure proteins were pooled, added with more TCEP to 2.0 mM, and concentrated prior to freezing and storage. However, equivalent attempts at eluting PDH failed due to insolubility. Full protein sequences are detailed in Supplemental Table 1.

Protein Cross-Linking and Identification

Proteins were cross-linked using disuccinimidyl glutarate (DSG, Thermo Fisher, which has a 7.7 Å spacer arm length) according to the manufacturer's recommendations. Briefly, 40 μg of each purified protein was reacted with 800 μg DSG in 450 mL pH 7.2 PBS, either alone or in pairs. Reaction vials were incubated for 30 min at room temperature. Cross-linker reaction was quenched with 50 mL 10x Tris-glycine buffer. Samples (1−2 μg) were then run in SDS-PAGE (50 min elution time, 200 V). Protein bands sent for proteomic analysis were subjected to in-gel digestion in triplicate.

Liquid Chromatography with Tandem Mass Spectroscopy for Proteomics

The peptides were separated and analyzed using a Vanquish Neo UHPLC System coupled to an Orbitrap Exploris 480 (Thermo Fisher Scientific, MA, USA) (n = 3 for each protein band). Separation was performed on an EASY-Spray 75 μm × 15 cm column packed with PepMap Neo C18 2 μm, 100 Å (Thermo Fisher Scientific) using solvent A (0.1% formic acid) and solvent B (0.1% formic acid in 80%

https://doi.org/10.1021/acsomega.6c00555
ACS Omega 2026, 11, 33872−33880

ACN) at a flow rate of 300 nL/min with a 60 min gradient. Peptides were then analyzed on an Orbitrap Exploris 480 apparatus with an EASY nanospray source (Thermo Fisher Scientific) at an electrospray potential of 2.0 kV. Raw data files were processed and searched using Proteome Discoverer 2.2 (Thermo Fisher Scientific). The Mascot algorithm was then used for data searching to identify proteins. Specific post-translational modifications (lysine acetylation, methionine oxidation, tryptophan oxidation, lysine trimethylation, proline phosphorylation, cysteine carboxyamidomethylation, cysteine proprioamidylation, and lysine monolinked with DSG) were also added as search options. Listed peptides (Table S3) were detected in at least 2 of 3 replicates.

In Silico Prediction of Protein Complexes

Protein complexes were predicted using AlphaFold 3.[17,19] Detected post-translational modifications from proteomics (lysine acetylation, trimethylation, and threonine phosphorylation) were used to constrain the prediction space, with default AlphaFold parameters. The protein sequences were restricted to those of the actual proteins (Table S1), prior to the addition of polyhistidine tagging and other additions during protein purification.[20] Please confirm the insertion of this citation.

Chemostat-Based Growth and ^{13}C-Glucose Labeling of *P. megaterium* SR7

P. megaterium SR7 was cultivated in quadruplicate using a laboratory-scale chemostat with a working volume of 280 mL. Modified Furch media (0.106 g $MgCl_2{\cdot}6H2O$, 0.048 g K_2SO_4, 0.020 g $MnCl_2{\cdot}4H2O$, 2.920 g NaCl, 0.747 g KCl, 2.000 g $(NH_4)_2SO_4$, 0.014 g $FeSO_4{\cdot}7H2O$, 3.520 g KH_2PO_4, 7.260 g $Na_2HPO_4{\cdot}2H_2O$) at pH 7 was used, 1 g/L glucose. The chemostats were stirred at 300 rpm and maintained at 37 °C using a heating jacket. The pH ranged between 6.7 and 7.0, while the oxidation−reduction potential (ORP) varied between 75 and 250 mV during cultivation. Aeration was provided using two Hailea ACO-5503 pumps, each supplying filtered air (0.22 μm Acrodisc) to two vessels, with air bubbled to the bottom of the vessels at 1.5 L/min. Inoculated chemostats were run at a dilution rate of 0.7 mL/min for at least four hydraulic retention times (28 h) to reach pseudosteady-state. For isotopic labeling, the medium was replaced with an equivalent glucose-labeled medium (40% [1,2-^{12} C_2] glucose, 20% [U-^{13} C_6] glucose, 40% unlabeled glucose), and cells were harvested after one additional hydraulic retention time.

LC-MS/MS Detection of Labeled Metabolites

To obtain cell extracts, cell pellets from 10 mL culture volume were first lysed via bead beater (0.1 mm silica beads) under 800 μL prechilled 50% methanol as quenching solution. Lysed samples were then transferred into new tubes and brought up to a total volume of 1.5 mL in 50% methanol. TCA cycle organic acids were measured using a derivatization based on 3-nitrophenylhydrazone and 1-ethyl-3-(3-(dimethylamino)propyl) carbodiimide (Han et al.), which allows quantitation of glycolate, lactate, malate, fumarate, succinate, citrate, isocitrate, pyruvate, oxaloacetate, and α-ketoglutarate. A Waters XEVO TQ-S was used to measure the MRM transitions. Isotopomer abundances were corrected for natural isotopic abundances using IsoCorrectoR.[21]

RESULTS

Co-Elution of PPC, PYK, and NDME Suggest Protein−Protein Interactions

Purified recombinant proteins of major enzymes (lactate dehydrogenase (LDH), NADH-dependent malic enzyme (NDME), phosphoenolpyruvate carboxylase (PPC), and pyruvate kinase (PYK)) surrounding the pyruvate node were obtained as previously described. Proteins were subjected to His-tag affinity chromatography as well as subsequent size exclusion chromatography.

Two major bands were observed for purified recombinant PPC (as opposed to single bands for purified recombinant LDH, NDME, and PYK), indicating either a potential proteolytic fragment or coeluting proteins associated with PPC, with an approximate molar weight between 60 and 70 kDa (Supporting Information, Figure 1A). Subsequent LC-MS-based proteomics confirmed the presence of both PYK and NDME (approximately 64.4 and 66.0 kDa, respectively) but not LDH in this protein band. Since coelution of proteins strongly suggests interaction between one or more of these proteins,[22] we inferred the possibility of PPC−PYK and PPC−NDME protein−protein interactions.

Protein Complexes Are Observed after DSG Cross-Linking

The addition of the DSG cross-linker encourages stable binding between proteins, causing predictable mass shifts. On the basis of observed mass shifts on SDS-PAGE, dimeric forms of PPC, LDH, and NDME in addition to tetrameric forms of LDH and PYK were observed. These observations corroborate previous literature, with the tetrameric form of PYK being well conserved across multiple phylogenetic groups,[23] while PPC and NDME have been observed in both dimeric and tetrameric forms.[24,25] The simultaneous formation of both dimeric and tetrameric LDH is also notable, as different isoforms may have different kinetics or regulatory properties.[26−28]

DSG cross-linking between different proteins was also tested in pairs. Selected SDS-PAGE gel bands were subjected to proteomics to confirm their identities. The presence of an LDH tetramer or dimer interaction (Supporting Information, Figure 1B and C) with a PYK tetramer, and an NDME monomer with a PYK monomer (Supporting Information, Figure 1D) interaction, was confirmed with subsequent proteomic analyses (Supporting Information Tables S2 and S3). These interactions between different proteins resulted in distinct molecular weight bands and proteomic signatures that were not present when each individual protein was cross-linked with only itself, suggesting interaction between the protein pairs. Unfortunately, the coelution of multiple enzymes simultaneously with purified PPC did complicate further analyses using PPC as an interaction partner, limiting conclusions that could be drawn. Additionally, aggregation of high-molecular-weight complexes in the wells could be observed (Supporting Information, Figure 1E), indicating likely nonspecific interactions[15] between all proteins.

In Silico Predictions of Protein Complexes

Predictions of potential protein−protein interactions were obtained using AlphaFold 3.0.[17,29] Predictions with only the protein sequences and without post-translational modifications (PTMs) failed to predict a feasible, stable interaction. Therefore, PTMs (other than the artificially induced monolinked DSG) detected in proteomics were also used to constrain the prediction space (Table 1).

A summary of the predicted protein complexes is detailed in Figure 2, alongside the predicted template modeling (pTM), interface predicted template modeling (ipTM), and predicted aligned error (PAE) scores. Predicted structures generally suggested a more accurate global structure prediction (pTM > 0.5), while the interfacing of the subunits within the global structure was subjected to a greater degree of uncertainty (ipTM < 0.6). In part, this may be because of a higher degree of disorder or accessory domains,[30] which would be expected for proteins that can interact with multiple targets, as may be the case for the tested proteins, and for dynamic metabolons.

https://doi.org/10.1021/acsomega.6c00555
ACS Omega 2026, 11, 33872−33880

Table 1. Detected Post-Translational Modifications from *P. megaterium* SR7 Proteomic Analyses Used to Constrain *In Silico* Predictions

Protein	Mass Shift (Th)	Post-Translational Modifications	Residues
PPC	+42.01	Acetylation	K21, K276, K287, K337, K483
	+42.05	Trimethylation	K173
	+114.03	Monolinked DSG[a]	K166, K182, K309, K337, K483, K609
LDH	+42.01	Acetylation	K8, K11, K46, K103, K232
	+42.05	Trimethylation	K72
	+114.03	Monolinked DSG[a]	K46, K232
NDME	+42.01	Acetylation	K9, K17, K19, K35, K66, K74, K209, K254, K293, K366, K372, K425, K432, K531, K535, K548, K556
	+42.05	Trimethylation	K361, K485, K523, K552
	+114.03	Monolinked DSG[a]	K9, K19, K35, K66, K297, K535, K567
PYK	+42.01	Acetylation	K59, K68, K145, K153, K155, K156, K272, K491, K496, K504
	+42.05	Trimethylation	K391, K486
	+79.97	Phosphorylation	T57, T60, T276, T278
	+114.03	Monolinked DSG[a]	K55, K68, K209, K265, K391, K479, K496, K504

[a]Monolinked DSG modifications were observed after treatment with DSG and were not used to constrain *in silico* predictions.

We additionally scanned for potential interacting interfacial residues in the best-case predictions by making use of the detected post-translational modifications, which have a potential to form cross-links,[15] spaced within less than 20 Å of each other (Figure 3). According to these predictions, the interfacing between PYK−PPC and NDME−PPC complexes may both be mediated by PPC(ALY287) and PPC(ALY276) residues, implying that that PPC cannot easily bind to both PYK and NDME simultaneously. In NDME−PPC, additional interactions between NDME(M3L552) or NDME(ALY9) with PPC(ALY337) were also observable. In LDH−PYK, potential interactions between PYK(ALY153) and LDH-(ALY8) or LDH(ALY11) were observed. In NDME−PYK, NDME(M3L552) and NDME(ALY548) were potential interaction partners with PYK(TPO57) and PYK(K55).

^{13}C Glucose Labeling Demonstrate Dilution of Metabolites and Potential Metabolon Formation

When subjected to enriched isotopic carbon labeling experiments in a chemostat environment where ^{13}C-labeled glucose (40% [1,2-^{1,3} C_2] glucose, 20% [U-$^{1\,3}$ C_6] glucose, 40% unlabeled glucose) is fed directly to the growth culture,[31] metabolites become enriched in ^{13}C, which is observable under LC-MS/MS. The differences in carbon enrichment between metabolically adjacent metabolites can often indicate the formation of metabolons,[32] which enhance reaction rates while shielding intermediates from competing pathways. Alternatively, differences in carbon enrichment can also arise from compartmentalized reactions occurring at different rates in different compartments. However, *P. megaterium* SR7 is a prokaryotic bacterium lacking membrane-bound organelles, making metabolite channeling from metabolon formation a more likely explanation. Most metabolites around the pyruvate node are notable for participating in multiple reactions, thus making their carbon enrichment highly variable. However, lactate, which is a waste product present in spent cell culture media, is primarily a product of the lactate dehydrogenase reaction.[33] Therefore, direct comparison of carbon enrichment of pyruvate and lactate is a relatively tractable indicator of metabolite dilution characteristic of metabolon formation. With no metabolite channeling or partitioning, the carbon labeling of lactate would be expected to be similar or less than the labeling of pyruvate. However, in *P. megaterium* SR7, significant differences ($p < 0.001$, Mann−Whitney U-test) in carbon enrichment were observed in pyruvate and lactate (Figure 4, Supplemental Figure 2A), with significantly more labeling of lactate as compared to pyruvate. Pyruvate and lactate originating from glycolysis generally maintains its carbon labeling due to the stoichiometry of glycolytic reactions, which produces two pyruvate per unit of glucose, while pyruvate sourced from anaplerotic reactions would have greater amounts of carbon scrambling. Glycolysis is typically an irreversible pathway, and subsequent lactate production is exported as waste product in *P. megaterium* SR7, making carbon scrambling from reversible reactions a less likely explanation. Examining the isotopomer distribution of pyruvate and lactate revealed a particularly enhanced labeling of M+2 and M+3 lactate isotopomers relative to pyruvate isotopomers, which were indicative of channeling of carbon to lactate directly from glycolysis given the enrichment of glucose in this labeling experiment, as opposed to from an anaplerotic route. Notably, metabolic flux analysis failed to converge on a fluxomic solution without allowances for isotopic dilution around the pyruvate node, which is characteristic of inactive metabolite pools or metabolon formation.[31] Moreover, as the measured intracellular concentrations of pyruvate (0.579 ± 0.198 mg/gDW) and lactate (0.656 ± 0.387 mg/gDW) were comparable, these differences in labeling also could not be explained merely by differences in pyruvate and lactate pool sizes. This observation therefore strongly suggested the *in vivo* formation of one or more metabolons surrounding the pyruvate node over other competing explanations.

Although our primary focus was the pyruvate node, ^{13}C labeling patterns in other central metabolites suggest additional metabolically channeled interactions that merit attention. We observed differences in carbon enrichment in metabolites within and surrounding the TCA cycle. A separate CO_2 fixation pathway involved in *P. megaterium* SR7 is the carbamoyl phosphate synthetase reaction, which produces citrulline and is heavily involved in the urea cycle. ^{13}C enrichment of citrulline (Citr) is among the highest of all measured metabolites (Figure 4, Supporting Information, Figure 2D), indicating heavy activity of carbamoyl phosphate synthetase. When operating solely in the urea cycle, citrulline will not accumulate any labeled carbon because the labeled carbon on citrulline is eventually lost after the arginase reaction, so the evidence instead suggested that the urea cycle is tied to the TCA cycle. For example, the urea cycle can be connected to the TCA cycle via the arginosuccinate synthetase pathway, interfacing with fundamental central carbon metabolism (Figure 5A). Carbon can also be transferred from the urea cycle after the interconversion of ornithine to glutamine and eventually AKG from the activity of ornithine aminotransferase (Figure 5B).

Interestingly, the observed carbon enrichment of succinate (Suc) also appears to be higher than that of α-ketoglutarate (AKG), and the labeling of succinate (Supplemental Figure 2B) partially resembles that of citrulline, raising the possibility

https://doi.org/10.1021/acsomega.6c00555
ACS Omega 2026, 11, 33872−33880

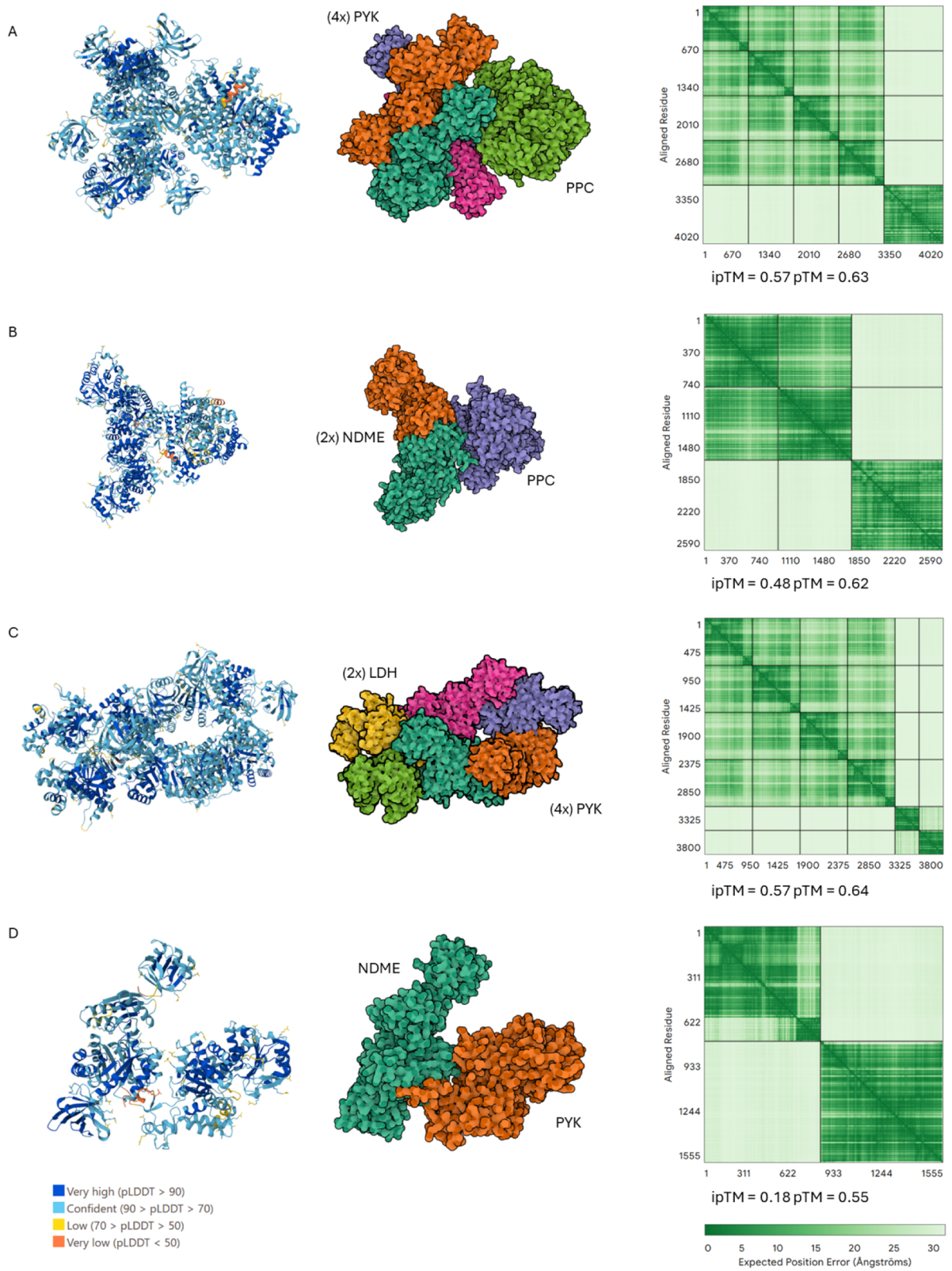

Figure 2. Predicted best-fit protein complexes by AlphaFold 3 for A) PPC−PYK tetramer, B) PPC−NDME dimer, C) LDH dimer−PYK tetramer, and D) NDME−PYK complexes. From left to right, figures indicate the ribbon model colored by predicted local distance difference test (pLDDT) score, the illustrative space-filling model, and the matrix of predicted aligned error (PAE) for each respective protein complex model.

that succinate formation is tied to the activity of a fumarate reductase or the reverse activity of succinate dehydrogenase, as opposed to the typical direction of α-ketoglutarate dehydrogenase/succinyl-CoA dehydrogenase. These differences in carbon enrichment again may implicate the formation of one or more potential metabolons surrounding the TCA cycle or the urea cycle. Previous evidence for metabolons in the urea cycle[34] generally suggests mitochondrial involvement, so a

https://doi.org/10.1021/acsomega.6c00555
ACS Omega 2026, 11, 33872−33880

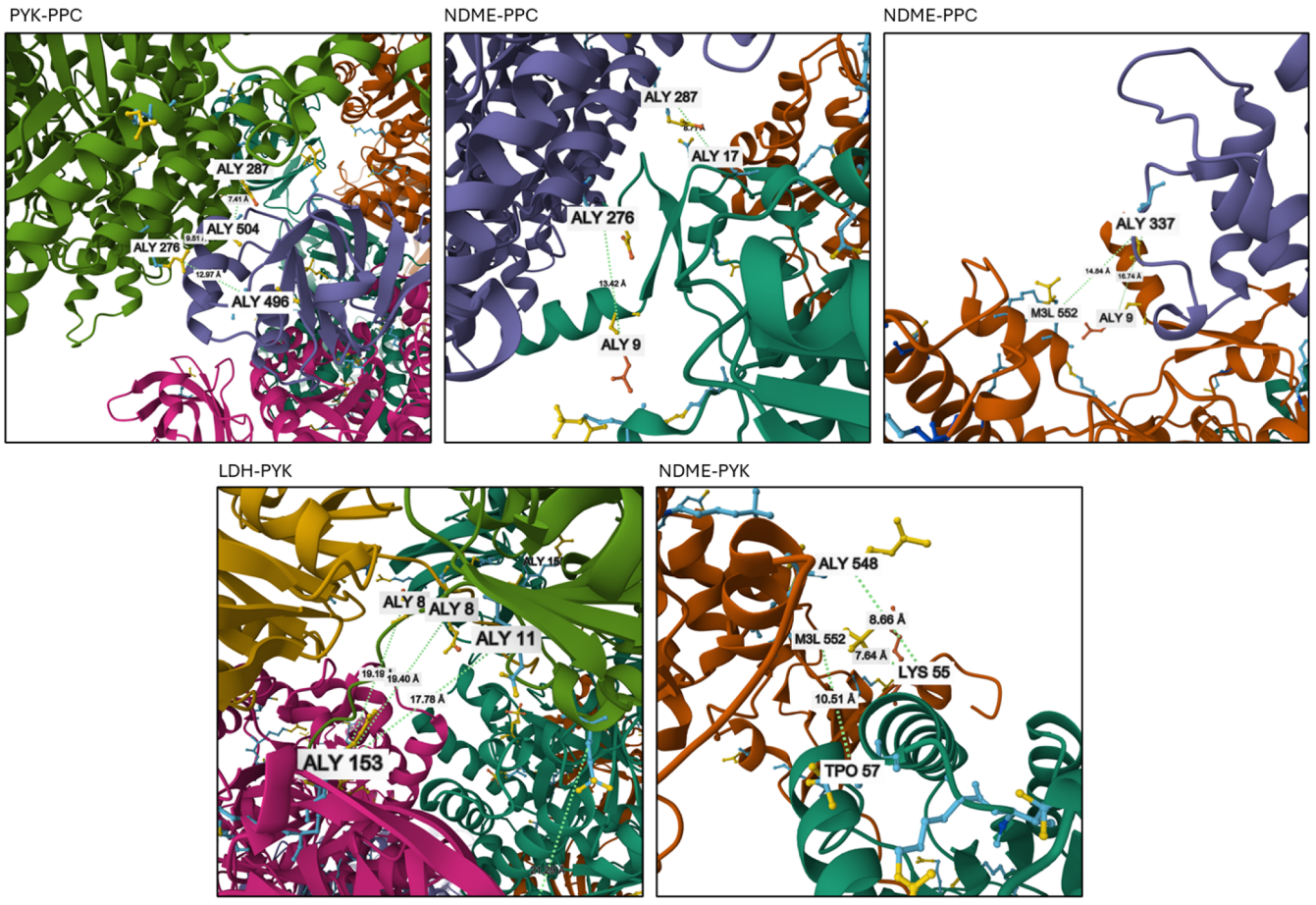

Figure 3. Potential protein−protein interacting residues for the best-fit protein complexes (Abbreviations: acetylated lysine ALY, trimethylated lysine M3L, phosphorylated threonine TPO).

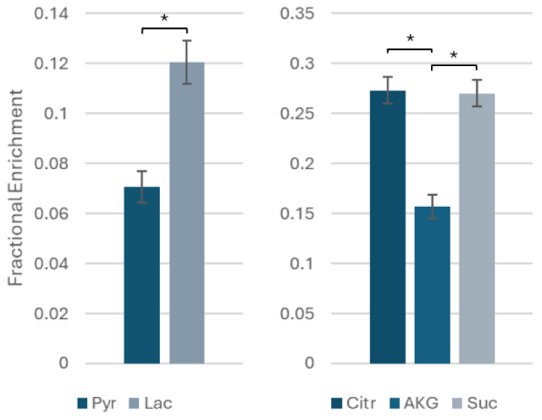

Figure 4. Fractional ^{13}C enrichment ($^{13}C/[^{12}C+^{13}C]$ after correction for naturally occurring ^{13}C) of metabolites associated with carbon flow through the central carbon metabolism (n = 3 independent bioreactors; error bars indicate standard deviation). The left panel shows pyruvate (Pyr) and lactate (Lac), and the right panel shows citrate (Citr), α-ketoglutarate (AKG), and succinate (Suc). The distinct isotopic incorporation patterns reveal dilution of labeled intermediates, consistent with potential channeling of metabolites between enzymes (* $p < 0.001$, Mann−Whitney U-test).

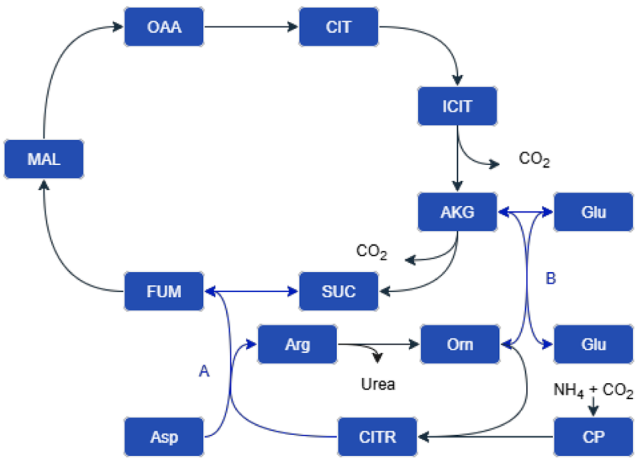

Figure 5. Simplified reaction diagram indicating interfacing between the urea cycle and the TCA cycle via A) arginosuccinate synthetase and B) ornithine aminotransferase, highlighting tentative carbon flux routes between the two cycles supported by isotopic labeling data.

metabolon forming without the need of a mitochondrial membrane is of particular interest, which can be explored in future work.

DISCUSSION

The *in vivo* formation of metabolons is difficult to characterize because of their dynamic and transient nature. Individual *in silico* predictions of protein−protein interactions alone do not constitute sufficient evidence of active formation under native conditions. Notably, as the proteins were expressed hetero-

https://doi.org/10.1021/acsomega.6c00555
ACS Omega 2026, 11, 33872−33880

logously in *E. coli* BL21, their post-translational modifications (PTMs) and subsequent interactions may not fully reflect the native PTM state in *P. megaterium* SR7. The detected PTMs should thus be regarded as tentative and may influence the *in silico* prediction. Similarly, *in vitro* cross-linking experiments demonstrate mass shifts consistent with binding between proteins but do not confirm their activity. The cross-linking data alone support the idea of interaction between protein pairs but could not resolve specific interprotein contact sites. The detection of isotopic labeling inconsistent with free diffusion demonstrated the potential for *in vivo* metabolon formation but did not elucidate the actual protein−protein interactions involved. However, by combining multiple lines of evidence, we reinforce the hypothesis that potential metabolon formations can occur around the pyruvate node in *P. megaterium* SR7 while excluding less likely hypotheses.

Since *in silico*, *in vitro*, and *in vivo* evidence all substantiate the formation of metabolons surrounding the pyruvate node, we must then question the functional or evolutionary purpose of these metabolons. Metabolon formation has been found to increase reaction rates by over 1 order of magnitude[35] even in synthetically constructed leaky metabolons; therefore, a general purpose for these metabolons is to accelerate central carbon metabolism.[36,37] However, the formation of metabolons is also often thought to be a reversible process that forms under specific conditions,[38] meaning that they can also serve regulatory or homeostatic functions. For example, when NAD+ production via lactate dehydrogenase is needed, the formation of LDH-PYK complexes will preferentially channel glycolytic carbon into lactate while shielding pyruvate from competing pathways. Alternatively, when TCA cycle metabolites are needed, the formation of the NDME-PYK complex can channel carbon between glycolysis and the TCA cycle. Additionally, the PPC-NDME complex is notable because NDME releases CO_2, whereas PPC fixes CO_2 as a substrate. As observed in cyanobacteria and plants that form carbonic anhydrase and RuBisCO metabolons, pairing CO_2 releasing and fixing reactions is a proven strategy to mitigate the diffusion of CO_2 and enhance otherwise slow kinetics.[14] In the context of *P. megaterium* SR7, which natively are adapted to elevated CO_2 partial pressures, regulatory mechanisms increasing the efficiency of CO_2 scavenging or fixating reactions may provide even greater return on investment than as compared to other nonextremophilic organisms.

Moreover, since *P. megaterium* SR7 lacks mitochondrial or other compartments, it is comparatively difficult to exert substrate-level control of enzymatic reactions, since neither metabolites nor enzymes can be segregated into different compartments. Without metabolons, increasing the level of pyruvate would simultaneously affect the rate of multiple different reactions, which is detrimental from a metabolic control perspective. The presence of metabolons may allow for significantly more fine-tuned control[38] across the pyruvate node. It is possible that these interactions are mediated by post-translational modifications.[39] However, the exact conditions affecting the formation of these protein−protein interactions are as yet unclear and are a consideration for future work.

CONCLUSIONS

This work revealed that the organization of central carbon metabolism in *P. megaterium* SR7 could extend beyond classical enzyme regulation, involving metabolon assemblies surrounding the pyruvate node that add a new dimension to metabolic control and engineering potential. The combined *in vitro*, *in silico*, and *in vivo* evidence suggested that these potential metabolons can channel metabolites in different metabolic directions, therefore presenting an additional potential regulatory mechanism. Co-elution and DSG cross-linking combined with proteomics suggested protein−protein interactions such as PPC−PYK, PPC−NDME, LDH−PYK, and NDME−PYK, which were supported by *in silico* predictions of feasible protein−protein interactions. Complementary *in vivo* ^{13}C labeling showed higher carbon enrichment in lactate than pyruvate, strongly supporting the presence of one or more metabolons surrounding the pyruvate node. These metabolons present additional metabolic engineering challenges and opportunities, since enhancing or disabling the formation of these metabolons could alter the central carbon metabolism of *P. megaterium* SR7. Alternatively, introducing these metabolons into other organisms could potentially allow for more fine-tuned metabolic control of glycolytic carbon flow, which is useful for future metabolic engineering purposes.

ASSOCIATED CONTENT

Data Availability Statement

Data are available throughout the manuscript and in the supplementary files. All data are also available upon request from the corresponding author.

Supporting Information

The Supporting Information is available free of charge at https://pubs.acs.org/doi/10.1021/acsomega.6c00555.

Figure S1: SDS-PAGE with purified and DSG cross-linked proteins. Table S1: Sequences of purified and recombinant proteins. Table S2: Summary of proteomic information across selected SDS-PAGE bands. Table S3: Peptides and associated post-translational modifications detected across selected SDS-PAGE bands. Figure S2: Mass isotopomer distributions for pyruvate, lactate, succinate, α-ketoglutarate, and citrulline (PDF)

PTMS data files (ZIP)

AUTHOR INFORMATION

Corresponding Author

Janelle R. Thompson − *Singapore Centre for Environmental Life Sciences Engineering, Nanyang Technical University, Singapore 637551, Singapore; Asian School of the Environment, Nanyang Technological University, Singapore 639798, Singapore*; Email: janelle.thompson@ntu.edu.sg

Authors

Nathaphon Yu King Hing − *Singapore Centre for Environmental Life Sciences Engineering, Nanyang Technical University, Singapore 637551, Singapore; Lee Kong Chian School of Medicine, Nanyang Technical University, Singapore 636921, Singapore*; orcid.org/0000-0002-7975-9399

Yi Wen Kristy Chang − *Singapore Centre for Environmental Life Sciences Engineering, Nanyang Technical University, Singapore 637551, Singapore; Asian School of the Environment, Nanyang Technological University, Singapore 639798, Singapore*

Ramanujam Srinivasan Vethathirri − *Singapore Centre for Environmental Life Sciences Engineering, Nanyang Technical University, Singapore 637551, Singapore; Asian School of the*

https://doi.org/10.1021/acsomega.6c00555
ACS Omega 2026, 11, 33872−33880

Environment, Nanyang Technological University, Singapore 639798, Singapore

Yulan Wang − *Lee Kong Chian School of Medicine, Nanyang Technical University, Singapore 636921, Singapore;* orcid.org/0000-0002-2831-8737

Complete contact information is available at: https://pubs.acs.org/10.1021/acsomega.6c00555

Notes

The authors declare no competing financial interest.

■ ACKNOWLEDGMENTS

This research was supported by the Singapore Ministry of Education under Academic Research Fund Tier 2 (MOE-T2EP30122-0015) and by the Singapore Ministry of Education and National Research Foundation through an RCE award to Singapore Centre for Environmental Life Sciences Engineering (SCELSE). We thank the NTU Protein Production Platform (https://proteins.sbs.ntu.edu.sg/) for cloning and protein purification of LDH, NDME, PPC, and PYK. We would like to acknowledge the Mass Spectrometry Core Facility in the School of Biological Sciences, Nanyang Technological University for their assistance with proteomic experiments.

■ REFERENCES

(1) Yen, H. W.; Hu, I. C.; Chen, C. Y.; Ho, S. H.; Lee, D. J.; Chang, J. S. Microalgae-Based Biorefinery − From Biofuels to Natural Products. *Bioresour. Technol.* **2013**, *135*, 166−174.

(2) Cho, J. S.; Kim, G. B.; Eun, H.; Moon, C. W.; Lee, S. Y. Designing Microbial Cell Factories for the Production of Chemicals. *JACS Au* **2022**, *2* (8), 1781−1799.

(3) Nielsen, J.; Keasling, J. D. Synergies between Synthetic Biology and Metabolic Engineering. *Nat. Biotechnol.* **2011**, *29* (8), 693−695.

(4) Freedman, A.; Peet, K.; Boock, J. T.; Penn, K.; Prather, K. L. J.; Thompson, J. R. Isolation, Development, and Genomic Analysis of Bacillus Megaterium SR7 for Growth and Metabolite Production Under Supercritical Carbon Dioxide. *Front Microbiol.* **2018**, *9*, 2152.

(5) Peet, K. C.; Freedman, A. J.; Hernandez, H. H.; Britto, V.; Boreham, C.; Ajo-Franklin, J. B.; Thompson, J. R. Microbial Growth under Supercritical CO2. *Appl. Environ. Microbiol.* **2015**, *81* (8), 2881−2892.

(6) Budisa, N.; Schulze-Makuch, D. Supercritical Carbon Dioxide and Its Potential as a Life-Sustaining Solvent in a Planetary Environment. *Life* **2014**, *4* (3), 331−340.

(7) Dassoff, E. S.; Li, Y. O. Mechanisms and Effects of Ultrasound-Assisted Supercritical CO2 Extraction. *Trends Food Sci. Technol.* **2019**, *86*, 492−501.

(8) Del Valle, J. M.; De La Fuente, J. C. Supercritical CO2 Extraction of Oilseeds: Review of Kinetic and Equilibrium Models. *Crit. Rev. Food Sci. Nutr.* **2006**, *46* (2), 131−160.

(9) Boock, J. T.; Freedman, A. J. E.; Tompsett, G. A.; Muse, S. K.; Allen, A. J.; Jackson, L. A.; Castro-Dominguez, B.; Timko, M. T.; Prather, K. L. J.; Thompson, J. R. Engineered Microbial Biofuel Production and Recovery under Supercritical Carbon Dioxide. *Nat. Commun.* **2019**, *10* (1), 1−12.

(10) Sahena, F.; Zaidul, I. S. M.; Jinap, S.; Karim, A. A.; Abbas, K. A.; Norulaini, N. A. N.; Omar, A. K. M. Application of Supercritical CO2 in Lipid Extraction − A Review. *J. Food Eng.* **2009**, *95* (2), 240−253.

(11) Wu, Z.; Liang, X.; Li, M.; Ma, M.; Zheng, Q.; Li, D.; An, T.; Wang, G. Advances in the Optimization of Central Carbon Metabolism in Metabolic Engineering. *Microb. Cell Fact.* **2023**, *22* (1), 76.

(12) Sauer, U.; Eikmanns, B. J. The PEP—Pyruvate—Oxaloacetate Node as the Switch Point for Carbon Flux Distribution in Bacteria: We Dedicate This Paper to Rudolf K. Thauer, Director of the Max-Planck-Institute for Terrestrial Microbiology in Marburg, Germany, on the Occasion of His 65th Birthday. *FEMS Microbiol. Rev.* **2005**, *29* (4), 765−794.

(13) Obata, T. Metabolons in Plant Primary and Secondary Metabolism. *Phytochem. Rev.* **2019**, *18* (6), 1483−1507.

(14) Huffine, C. A.; Zhao, R.; Tang, Y. J.; Cameron, J. C. Role of Carboxysomes in Cyanobacterial CO2 Assimilation: CO2 Concentrating Mechanisms and Metabolon Implications. *Environ. Microbiol.* **2023**, *25* (2), 219−228.

(15) Wu, F.; Minteer, S. Krebs Cycle Metabolon: Structural Evidence of Substrate Channeling Revealed by Cross-Linking and Mass Spectrometry. *Angew. Chem. Int. Ed.* **2015**, *54* (6), 1851−1854.

(16) Bulutoglu, B.; Garcia, K. E.; Wu, F.; Minteer, S. D.; Banta, S. Direct Evidence for Metabolon Formation and Substrate Channeling in Recombinant TCA Cycle Enzymes. *ACS Chem. Biol.* **2016**, *11* (10), 2847−2853.

(17) Evans, R.; O'Neill, M.; Pritzel, A.; Antropova, N.; Senior, A.; Green, T.; Žídek, A.; Bates, R.; Blackwell, S.; Yim, J.et al.Protein Complex Prediction with AlphaFold-Multimer. *bioRxiv* **2022**. .

(18) Abernathy, M. H.; He, L.; Tang, Y. J. Channeling in Native Microbial Pathways: Implications and Challenges for Metabolic Engineering. *Biotechnol. Adv.* **2017**, *35* (6), 805−814.

(19) Abramson, J.; Adler, J.; Dunger, J.; Evans, R.; Green, T.; Pritzel, A.; Ronneberger, O.; Willmore, L.; Ballard, A. J.; Bambrick, J.; Bodenstein, S. W.; Evans, D. A.; Hung, C. C.; O'Neill, M.; Reiman, D.; Tunyasuvunakool, K.; Wu, Z.; Žemgulytė, A.; Arvaniti, E.; Beattie, C.; Bertolli, O.; Bridgland, A.; Cherepanov, A.; Congreve, M.; Cowen-Rivers, A. I.; Cowie, A.; Figurnov, M.; Fuchs, F. B.; Gladman, H.; Jain, R.; Khan, Y. A.; Low, C. M. R.; Perlin, K.; Potapenko, A.; Savy, P.; Singh, S.; Stecula, A.; Thillaisundaram, A.; Tong, C.; Yakneen, S.; Zhong, E. D.; Zielinski, M.; Žídek, A.; Bapst, V.; Kohli, P.; Jaderberg, M.; Hassabis, D.; Jumper, J. M. Accurate Structure Prediction of Biomolecular Interactions with AlphaFold 3. *Nature* **2024**, *630* (8016), 493−500.

(20) Han, J.; Gagnon, S.; Eckle, T.; Borchers, C. H. Metabolomic Analysis of Key Central Carbon Metabolism Carboxylic Acids as Their 3-Nitrophenylhydrazones by UPLC/ESI-MS. *Electrophoresis* **2013**, *34* (19), 2891−2900.

(21) Heinrich, P.; Kohler, C.; Ellmann, L.; Kuerner, P.; Spang, R.; Oefner, P. J.; Dettmer, K. Correcting for Natural Isotope Abundance and Tracer Impurity in MS-, MS/MS- and High-Resolution-Multiple-Tracer-Data from Stable Isotope Labeling Experiments with IsoCorrectoR. *Sci. Rep.* **2018**, *8* (1), 17910.

(22) Salas, D.; Stacey, R. G.; Akinlaja, M.; Foster, L. J. Next-Generation Interactomics: Considerations for the Use of Co-Elution to Measure Protein Interaction Networks. *Mol. Cell. Proteomics* **2020**, *19* (1), 1−10.

(23) Morgan, H. P.; Zhong, W.; McNae, I. W.; Michels, P. A. M.; Fothergill-Gilmore, L. A.; Walkinshaw, M. D. Structures of Pyruvate Kinases Display Evolutionarily Divergent Allosteric Strategies. *R. Soc. Open Sci.* **2014**, *1* (1), 140120.

(24) Kai, Y.; Matsumura, H.; Izui, K. Phosphoenolpyruvate Carboxylase: Three-Dimensional Structure and Molecular Mechanisms. *Arch. Biochem. Biophys.* **2003**, *414* (2), 170−179.

(25) Hsieh, J. Y.; Chen, S. H.; Hung, H. C. Functional Roles of the Tetramer Organization of Malic Enzyme. *J. Biol. Chem.* **2009**, *284* (27), 18096−18105.

(26) Tenenbaum-Bayer, H.; Levitzki, A. The Refolding of Lactate Dehydrogenase Subunits and Their Assembly to the Functional Tetramer. *Biochim. Biophys. Acta - Enzymol.* **1976**, *445* (2), 261−279.

(27) Yamamoto, S.; Storey, K. B. Influence of glycerol on the activity and tetramer-dimer state of lactate dehydrogenase isozymes. *Inr. J. Biochem.* **1988**, *20*, 1267−1271.

(28) Jackson, R. M.; Gelpi, J. L.; Cortes, A.; Emery, D. C.; Wilks, H. M.; Moreton, K. M.; Halsall, D. J.; Sleigh, R. N.; Behan-Martin, M.; et al. Construction of a Stable Dimer of Bacillus Stearothermophilus Lactate Dehydrogenase. *Biochemistry* **1992**, *31* (35), 8307−8314.

(29) Omidi, A.; Møller, M. H.; Malhis, N.; Bui, J. M.; Gsponer, J. AlphaFold-Multimer Accurately Captures Interactions and Dynamics

of Intrinsically Disordered Protein Regions. *Proc. Natl. Acad. Sci. U. S. A.* **2024**, *121* (44), No. e2406407121.
(30) Dunbrack, R. L., Jr. Rēs ipSAE loquuntur: What's wrong with AlphaFold's ipTM score and how to fix it. *bioRxiv* **2025**. DOI: 10.1101/2025.02.10.637595
(31) Chang, K. Y. W.; Song, Y.; Yu King Hing, N.; Vethathirri, R. S.; Wang, Y.; Thompson, J. R. Growth-resolved genome-scale metabolic modeling of Priestia megaterium SR7 validated by chemostat and 13-C flux analysis. *bioRxiv* **2026**, DOI: 10.64898/2026.05.27.728139.
(32) Omini, J.; Dele-Osibanjo, T.; Kim, H.; Zhang, J.; Obata, T. Is the TCA Cycle Malate Dehydrogenase-Citrate Synthase Metabolon an Illusion? *Essays Biochem.* **2024**, *68* (2), 99−106.
(33) Wu, K.; Mao, Z.; Mao, Y.; Niu, J.; Cai, J.; Yuan, Q.; Yun, L.; Liao, X.; Wang, Z.; Ma, H. EcBSU1: A Genome-Scale Enzyme-Constrained Model of Bacillus Subtilis Based on the ECMpy Workflow. *Microorganisms* **2023**, *11* (1), 178.
(34) Watford, M. Channeling in the Urea Cycle: A Metabolon Spanning Two Compartments. *Trends Biochem. Sci.* **1989**, *14* (8), 313−314.
(35) You, C.; Zhang, Y. -H. P. Self-Assembly of Synthetic Metabolons through Synthetic Protein Scaffolds: One-Step Purification, Co-Immobilization, and Substrate Channeling. *ACS Synth. Biol.* **2013**, *2* (2), 102−110.
(36) Ranganathan, S.; Liu, J.; Shakhnovich, E. Enzymatic Metabolons Dramatically Enhance Metabolic Fluxes of Low-Efficiency Biochemical Reactions. *Biophys. J.* **2023**, *122* (23), 4555−4566.
(37) Wang, H.; Vant, J. W.; Zhang, A.; Sanchez, R. G.; Wu, Y.; Micou, M. L.; Luczak, V.; Whiddon, Z.; Carlson, N. M.; Yu, S. B.; Jabbo, M.; Yoon, S.; Abushawish, A. A.; Ghassemian, M.; Masubuchi, T.; Gan, Q.; Watanabe, S.; Griffis, E. R.; Hammarlund, M.; Singharoy, A.; Pekkurnaz, G. Organization of a Functional Glycolytic Metabolon on Mitochondria for Metabolic Efficiency. *Nat. Metab.* **2024**, *6* (9), 1712−1735.
(38) Imaizumi, R.; Waki, T.; Hattori, Y.; Takeshita, K.; Sumita, M.; Kawaguchi, K.; Kumeta, H.; Umeda, K.; Sato, K.; Yanai, T.; et al.. Transient Metabolon Dynamics Tune Enzyme Specificity. *ChemRxiv* **2025**. DOI: 10.26434/chemrxiv-2025-npkrm.
(39) Hong, X.; Li, N.; Lv, J.; Zhang, Y.; Li, J.; Zhang, J.; Chen, H. -F. PTMint Database of Experimentally Verified PTM Regulation on Protein−Protein Interaction. *Bioinformatics* **2023**, *39* (1), btac823.

https://doi.org/10.1021/acsomega.6c00555
ACS Omega 2026, 11, 33872−33880